Available online at www.sciencedirect.com
ScienceDirect
Journal of Power Sources 159 (2006) 149–154
JOURNAL OF POWER SOURCES
www.elsevier.com/locate/jpowsour

Short communication

Microstructure evaluations and hydrogenation properties on Ti–*x*Nb–10Cr alloys

Kyung Shin [a], Song Seok [a], Soon-Chul Ur [a], Young-Jig Kim [b], Tae-Whan Hong [a,*]

[a] *Research Center for Sustainable ECo-Device & Materials (ReSEM), Chungju National University, 123 Geomdan-ri, Iryu-myeon, Chungju, Chungbuk 380-702, Korea*
[b] *School of metall. and Mat. Eng., Sungkyunkwan University, Suwon 446-746, Korea*

Available online 5 June 2006

Abstract

Ti–Cr alloys consist of BCC solid solution, C36, C14, C15 Laves phase at high temperature. Among others, the BCC solid solution phase was reported to have a high hydrogen storage capacity. However, activation, wide range of hysteresis at hydrogenation/dehydrogenation, and degradation of hydrogen capacity due to hydriding/dehydriding cycles must be improved for its application. In this study, to improve such problems, we added a Nb. For attaining target material, Ti–1Nb–10Cr, Ti–3Nb–10Cr and Ti–5Nb–10Cr specimens were prepared by a planetary ball mill. The milling process was carried out under a high pressure nitrogen atmosphere. Specimens synthesized were characterized using X-ray diffraction (XRD), scanning electron microscopy (SEM) with energy dispersive spectroscopy (EDS), transmission electron microscopy (TEM) and thermogravimetric analysis/differential scanning calorimetry (TG/DSC). In order to examine hydrogenation behavior, a pressure-composition-isotherm (PCI) was performed at 323, 373, 423, 473 and 523 K.

Keywords: Hydrogenation properties; Ti–Cr alloy; Laves phase; Planetary ball mill

1. Introduction

In an ideal world, we might envision a future where electricity, heat and motive power are derived from renewable energy sources. Hydrogen could be a key player in certain applications as an energy storage medium in this future world. The density of hydrogen is so low at ambient temperatures and pressures that it is not practical to store under these conditions. There are several different ways to store hydrogen. Hydrogen can be stored as a gas or liquid or in a chemical compound using a variety of technologies. Compact storage of hydrogen gas in tanks in mature storage technology is difficult because hydrogen is the lightest element and has very low density under normal conditions. This is addressed through compression to higher pressures or interaction with other compounds. In addition, storage tank materials are advancing as they are getting lighter and better able to provide containment. Some have a protective outside layer to improve impact resistance and safety. Liquid hydrogen is stored in cryogenic containers, which requires less volume than gas storage. However, the liquefaction of hydrogen consumes large quantities of electric power, equivalent to about one-third the energy value of the hydrogen. Hydrogen can be stored "reversibly" and "irreversibly" in metal hydrides. In reversible storage, metals are generally alloyed to optimize both the system weight and the temperature at which the hydrogen can be recovered. When the hydrogen needs to be used, it is released from the hydride at a certain temperature and pressure and the alloy is restored to its previous state. In irreversible storage, the material undergoes a chemical reaction with another substance, such as water that releases the hydrogen from the hydride. The byproduct is not reconverted to a hydride [1].

In particular, Ti and Ti based hydrogen storage alloys have been thought to be the third generation of alloys with a high hydrogen capacity. However, it is difficult to treat activation. In order to solve the problem, activation, wide range of hysteresis at hydriding/dehydriding, and degradation of hydrogen capacity due to hydriding/dehydriding cycled must be improved for its application [2].

This study focused on Ti–Cr alloy. These alloys had a high capacity of approximately 0.8 wt.% [3,18]. Okada et al. reported that a meta-stable system could be stabilized by the addition of a third element such as V, Mo, Ta or Nb, etc. Especially, when

* Corresponding author.
E-mail address: twhong@chungju.ac.kr (T.-W. Hong).

0378-7753/$ – see front matter © 2006 Elsevier B.V. All rights reserved.
doi:10.1016/j.jpowsour.2006.04.017

added to Nb and Ta elements, it formed a Laves phase in this system [4–6]. On the other hand, Small et al. reported that hydrogen was absorbed during the ball milled titanium phase and the absorption rate was significantly greater than had been implied by the results of the experiments when the sample was milled under approximate constant hydrogen pressure conditions and when milling was interrupted to refill the vial with gas [7–10]. In this paper, we added Nb which refers to a previous study. Ti–Nb–Cr ternary alloy was prepared using a planetary ball mill kind of mechanical alloying (MA). We aimed to improve hydrogenation properties with activation [11,12].

2. Experimental

Fig. 1 shows the schematic diagram of an experimental procedure. The starting material for all experiments prepared Ti, Nb and Cr powder with a purity of 3N. The powders were mechanically alloyed for 140 hours with Cr steel ball. Mechanical alloying was performed using a laboratory planetary ball mill (FRITSCH co., Pulverisette-5) at 200 rpm at an ambient temperature. The powders were charged in an AISI 304 reactor of 45 cm^3 volume. The BPR (ball to powder ratio) was fixed at 40:1. After evacuating down, the high purity nitrogen gas of 5N was introduced to a reactor with 1 bar. After mechanical alloying,

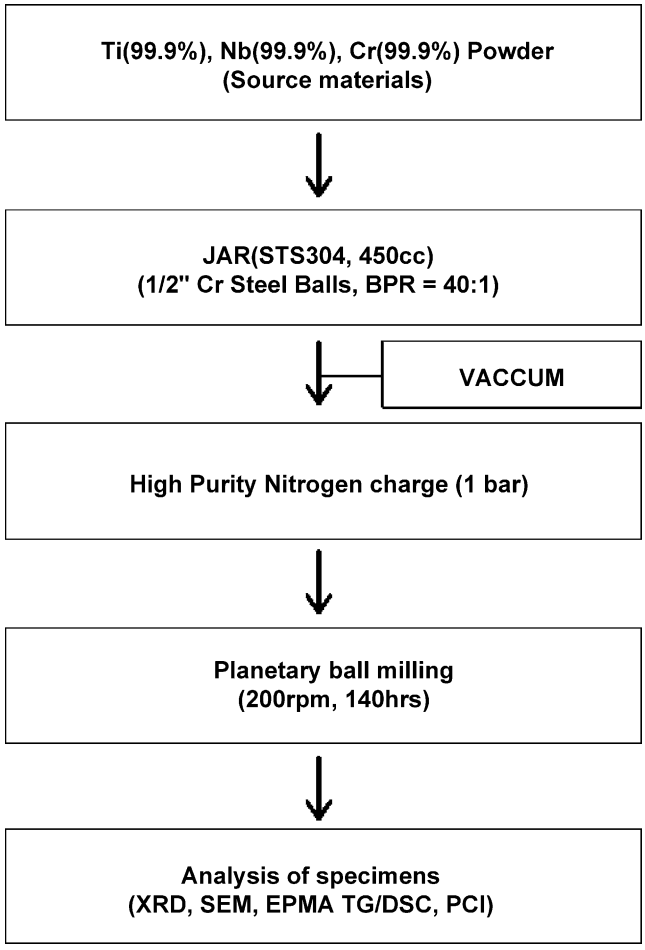

Fig. 1. Schematic diagram of experimental procedure.

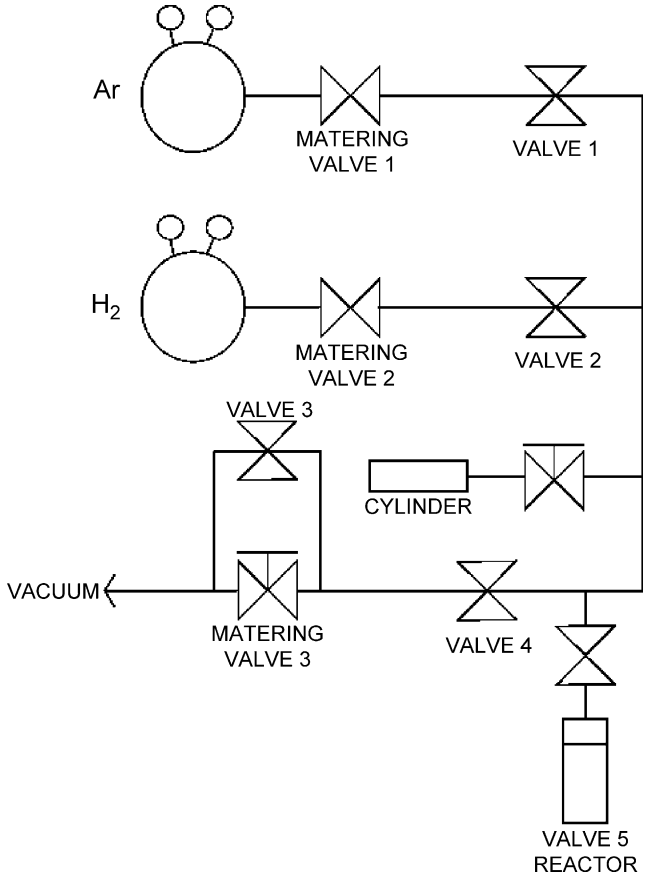

Fig. 2. Schematic diagram of Sievert's type automatic pressure-composition-isotherm apparatus.

all the prepared specimens were handled in a glove box filled with purified nitrogen to avoid the influence of oxidation and moisture. Mechanically alloyed particles were characterized by X-ray diffraction (XRD) pattern using a RINT-2000(RIGAKU Co., 1.5405 Å Cu Kα, 1° min^{-1}). Using thermogravimetric analysis/differential scanning calorimetry (TG/DSC) (NETZSCH Co., STA409PC-Luxx), thermogravity analysis was carried out under a pure argon atmosphere heated up to 1073 K at 5 K min^{-1}.

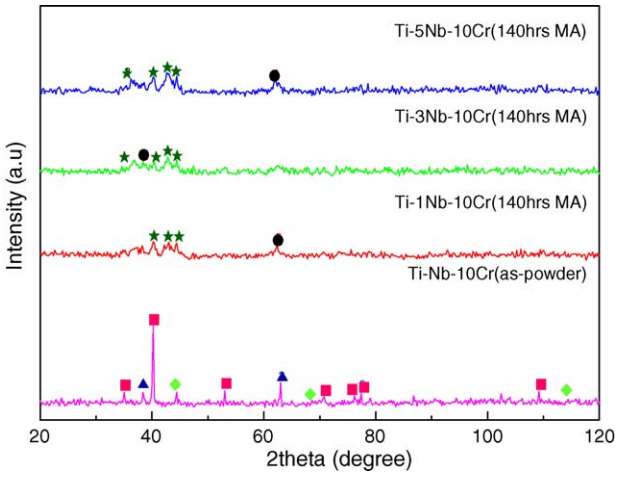

Fig. 3. Results of XRD analysis on Ti–*x*Nb–10Cr alloys.

The morphology and composition of the particles were observed using scanning electron microscopy (SEM) with energy dispersive spectroscopy (EDS). Microstructures of the particles were observed by transmission electron microscopy (TEM). Fig. 2 shows the schematic diagram of Seivert's type automatic pressure-composition-isotherm (PCI) apparatus. The hydriding properties were analyzed by Sievert's type automatic pressure-composition-isotherm apparatus at 323, 373, 423, 473 and 523 K.

3. Results and discussion

Fig. 3 shows the results of an XRD analysis on Ti–xNb–10Cr ($x = 1, 3, 5$) alloys after 140 hours of MA. After mechanical alloying, an oxidation peak which has a negative affect and impact on hydrogen storage was not observed. This was due to samples being exposed to nitrogen during mechanical alloying to prevent oxidation. Moreover, all peaks made completely broaden by formation of the phase made up of nanocrystalline and amorphous phases. As reported by Okada et al. [4–6], the addition of Nb on Ti–Cr systems consisted of mainly Laves phase besides the bcc phase. The size of the crystalline phase could be calculated with a Scherrer equation. The crystallite size of the specimen was measured at 40–140 μm.

Table 1 shows the crystallite size of Ti–xNb–10Cr ($x = 1$, 3, 5) alloys determined by XRD. Considering the composition of the sample, we expected to observe mainly Ti peak. However, according to the effect of amorphous or nanocrystallite, inten-

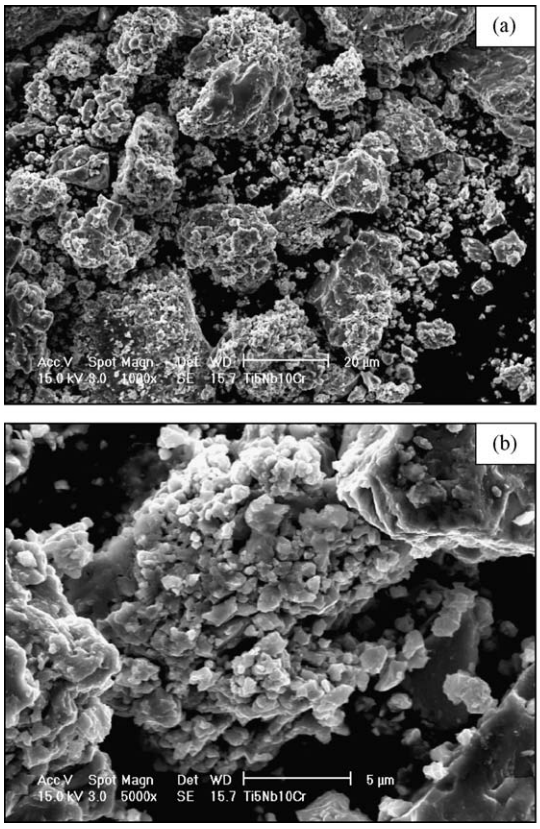

No.	ELE.	W.L (A)	PKI-BGI	SID (I)	I-Ratio	Mol (%)
1	Ti Ka	2.7485	104422.75	3904.02	2.6697	88.474
2	Nb La	5.7243	94.44	372.05	0.2538	5.196
3	Cr Ka	2.2897	115.91	620.45	0.1867	6.330

Fig. 4. Surface morphologies and nominal composition on Ti–5Nb–10Cr alloy.

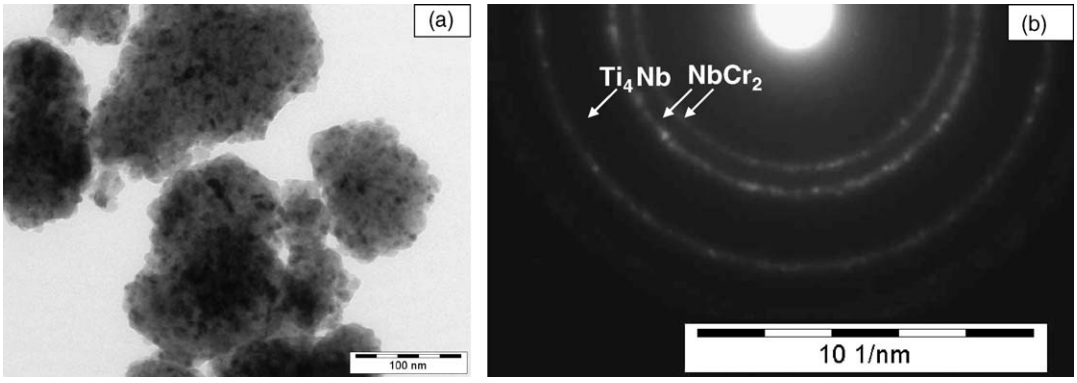

Fig. 5. TEM micrographs on Ti–5Nb–10Cr alloy about (a) bright field image; (b) SADP (selected area diffraction pattern).

Table 1
Crystallite size of Ti–*x*Nb–10Cr alloys determined by XRD

Ti–*x*Nb–10Cr (*x* = 1, 3, 5)	Crystalline size (nm)			
	$NbCr_2$ (hkl)	Scherrer	Ti_4Nb (hkl)	Scherrer
Ti–1Nb–10Cr	103	125.1	130	137.4
	220	126.3		
	112	126.9		
	201	85.1		
Ti–3Nb–10Cr	110	83	020	62.8
	103	126.1		
	220	84.6		
	112	63.4		
	201	85.1		
Ti–5Nb–10Cr	110	41.4	130	139.1
	103	83.8		
	200	63.3		
	112	84.7		
	201	63.4		

sity of Ti-related peaks became very weak. Otherwise, $NbCr_2$ peaks appeared preponderantly in the range of 30–50°. These alloys were estimated with an effect of AB_2-type phase, namely $NbCr_2$ [13–17] solid solution. As reported by Skipov et al. [13], Nb did not form any inter-metallic compound and $NbCr_2$ had a high mobility of hydrogen at a relatively low temperature. Maximum hydrogen capacity of $NbCr_2$ alloy was confirmed at approximately 0.9 wt.%. According to the reference in the previous study [18], we concluded that the target material was prepared successfully for improvement of the hydrogenation properties.

Fig. 4 shows the surface morphologies on Ti–5Nb–10Cr alloys after mechanically alloyed using SEM. The particles synthesized were composed of fine particles agglomerated at less than 5 μm. Agglomerated particles were discovered to be a size of approximately 10–40 μm. Accordingly, peaks of planetary ball milled specimens after 140 h was observed to have generally broadened. We confirmed that the milling time was optimal in this system. In addition to the results of the electron probe micro analysis (EPMA) analysis, all specimens were confirmed to harmonize with target materials.

Fig. 5 shows the micrographs on a Ti–5Nb–10Cr alloy: (a) bright field image and (b) selected area diffraction pattern (SADP) by using TEM. The average crystal sizes coincided with XRD results. The corresponding selected area diffraction pattern of the Ti–5Nb–10Cr alloy showed a continuous and broadening ring pattern, which indicated the coexistence of amorphous and nanocrystallline phases. Primary, second, and third diffraction patterns were reported as $NbCr_2$ and Ti_4Nb, respectively. Among the diffraction ring patterns, the partially spotty ring patterns were indicated by the *Mòir fringe* effect.

Fig. 6 shows the results of a DSC analysis after a hydriding evaluation at 423, 473 and 523 K. Table 2 shows the onset temperature in Ti–*x*Nb–10Cr (*x* = 1, 3, 5) alloys. There was no reaction at 423 K (a) and 473 K (a). The endothermic reactions in stages 1 and 2 seemed to occur at 473 K (b). Each onset temperature was recorded at 632.6 and 751.1 K, respectively. Also,

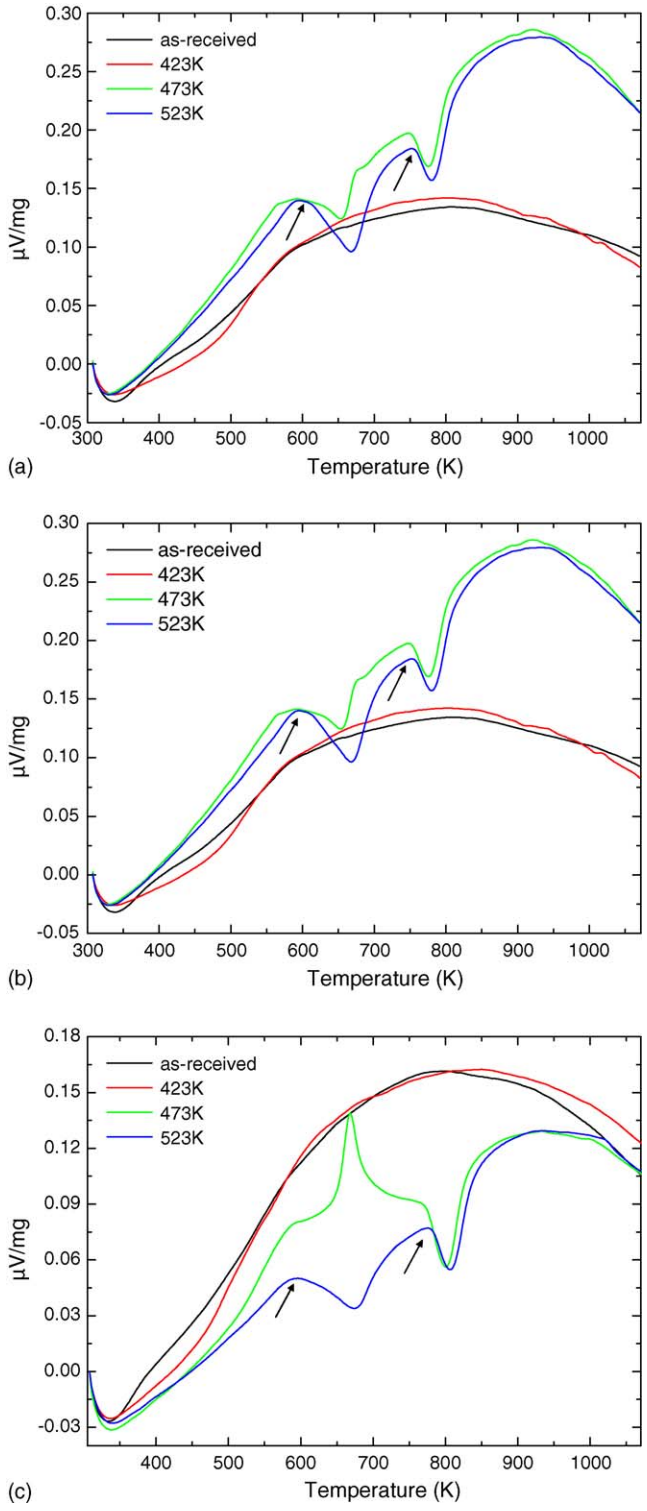

Fig. 6. Results of DSC experiment on (a) Ti–1Nb–10Cr; (b) Ti–3Nb–10Cr; and (c) Ti–5Nb-10Cr alloys.

the exothermic reaction of stage 1 and the endothermic reaction of stage 2 were recorded at 473 K (c). In 523 K, all samples revealed the endothermic of stages 1 and 2. Increasing the addition to Nb, the onset temperature of stage 1 was generated very quickly. In consequence, Ti–*x*Nb–10Cr (*x* = 1, 3, 5) alloys proceeded to phase transformation for the two steps.

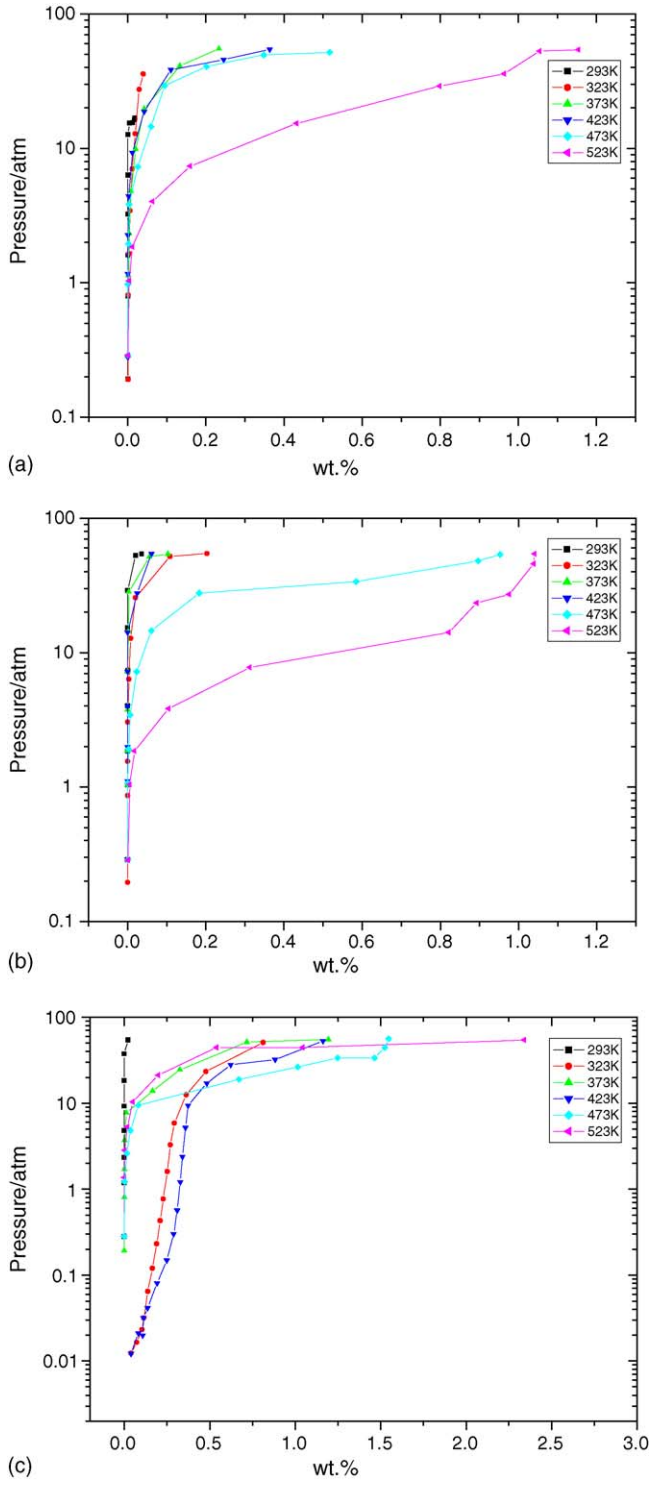

Fig. 7. Hydriding profiles of (a) Ti–1Nb–10Cr; (b) Ti–3Nb–10Cr; and (c) Ti–5Nb–10Cr alloys by using PCI.

Fig. 7 shows the hydriding profile of Ti–*x*Nb–10Cr ($x = 1, 3, 5$) alloys by using pressure-composition-isotherm. In PCI profiles, total hydriding reaction slope was difficult to observe in the phase ($\alpha + \beta$) coexistence region, namely for plateau pressure. In Ti–1Nb–10Cr alloy, hydrogen storage capacity was increased gradually to exceed 523 K. These results coincided with the tendency of Ti–3Nb–10Cr and Ti–5Nb–10Cr alloys. In addition, the reversible capacity in this system was approximately 0.81, 0.72 and 1.2 wt.%, respectively. The Ti–5Nb–10Cr alloy showed a full hydrogen capacity of approximately 2.34 wt.%. Therefore, Ti–*x*Nb–10Cr ($x = 1, 3, 5$) alloys with the addition of Nb is believed to be an excellent material for hydrogenation properties compared to that in the previous study [14–17].

Table 2
Onset temperature of Ti–*x*Nb–10Cr alloys

Temperature (K)	Onset temperature (K)		
	Ti–1Nb–10Cr	Ti–3Nb–10Cr	Ti–5Nb–10Cr
473	–	632.6	650.4
	–	751.1	800.4
523	615.7	596.6	594.3
	759.4	756.5	805.1

4. Conclusions

The main conclusions from this study are as follow:

1. In the XRD results, these alloys were calculated with the effect of an AB_2-type phase, namely an $NbCr_2$ solid solution. All peaks were completely broadened by formation of the phase made up of nanocrystalline and amorphous phases. Therefore, the target material was prepared successfully for the improvement of hydrogenation properties.
2. Accordingly, peaks of a planetary ball milled specimen after 140 h was observed as having generally broadened. These results coincided with the XRD analysis. In addition to the results of the EPMA analysis, all specimens were confirmed to harmonize with target materials.
3. The corresponding selected area diffraction pattern of the Ti–5Nb–10Cr alloy showed a continuous and broadening ring pattern, which indicated the coexistence of the amorphous and nanocrystallline phases. Among the diffraction ring patterns, the partially spotty ring patterns indicated by the *Mòir fringe* effect.
4. In the TG/DSC results, increasing the addition of Nb, the onset temperature of stage 1 generated very quickly. In consequence, Ti–*x*Nb–10Cr ($x = 1, 3, 5$) alloys proceeded to phase transformation for steps 1 and 2 using a hydrogenation process.
5. In the PCI analysis, the reversible capacity in this system was assigned values of approximately 0.81, 0.72 and 1.2 wt.%, respectively. The Ti–5Nb–10Cr alloy showed a full hydrogen capacity of approximately 2.34 wt.%. As a result, the Ti–*x*Nb–10Cr ($x = 1, 3, 5$) alloys with the addition of Nb was considered an ideal material for hydrogenation properties.

Acknowledgement

This research was supported by the Regional Innovation Center (RIC) Program, which was conducted by the Ministry of Commerce, Industry and Energy of the Korean Government.

References

[1] B. Johnston, M.C. Mayo, A. Khare, Technivation 25 (2005) 569–585.
[2] N. Takeichi, H. Senoh, H.T. Takeshita, T. Oishi, H. tanaka, T. Kiyobayashi, N. Kuriyama, Mater. Sci. Eng. B 108 (2004) 100–104.
[3] Y. Machiada, Hydride for Energy Source, Oxford, 1978, pp. 329–336.
[4] M. Okada, T. Kuriiwa, T. Tamura, H. Takamura, A. Kamegawa, Met. Mater. Int. 7 (2001) 67.
[5] M. Okada, T. Kuriiwa, A. Kamegawa, H. Takamura, Mater. Sci. Eng. A 329–331 (2002) 305–312.
[6] M. Okada, T. Chou, A. Kamegawa, T. Tamura, H. Takamura, A. Matsukawa, S. Yamashita, J. Alloys Compd. 356–357 (2003) 480–485.
[7] D.A. Small, G.R. MacKay, R.A. Dunlap, J. Alloys Compd. 284 (1999) 312–315.
[8] N. Takeichi, H.T. Takeshita, H. Tanaka, T. Kiyobayashi, N. Kuriyama, Mater. Lett. 57 (2003) 1395–1399.
[9] J.F. Fernandez, D.R. Sanchez, J. Alloys Compd. 330–332 (2002) 601–606.
[10] N. Takeichi, H. Senoh, H.T. Takechita, T. Oishi, H. Tanaka, T. Kiyobayashi, H. Kuriyama, Mater. Sci. Eng. B 108 (2004) 100–104.
[11] E. Kalaid, Current Topics in Materials Science, North-Holland Publishing Company, 1978, pp.603–651.
[12] J.Y. Lee, J.H. Kim, H.M. Lee, J. Alloys Compd. 297 (2000) 231–239.
[13] A.V. Skipov, A.L. Buzlukov, V.N. Kozhanov, T.J. Udovic, Q. Huang, J. Alloys Compd. 359 (2003) 27–34.
[14] A.Y. Esayed, D.O. Northwood, Int. J. Hydrogen Energy 22 (1) (1997) 77–82.
[15] A.Y. Esayed, Int. J. Hydrogen Energy 25 (2000) 357–362.
[16] A.Y. Esayed, Int. J. Hydrogen Energy 25 (2000) 363–368.
[17] A.Y. Esayed, D.O. Northwood, Int. J. Hydrogen Energy 20 (11) (1995) 893–896.
[18] http://hydpark.ca.sandia.gov/MaterialsFrame.html.